ACI MATERIALS JOURNAL TECHNICAL PAPER

Title No. 123-M27

Performance-Based Evaluation of Concrete Freezing-and-Thawing Considering Climate Change

by Jin-Su Kim, Woo-Ri Kwon, Norhazilan Md Noor, and Jang-Ho Jay Kim

Due to global warming, the temperature of the Earth's surface increased by 0.95 to 1.20°C in the past four decades. The increase in temperature has significant effects on the concrete industry, causing alternations in concrete curing conditions and degradation in strength and durability properties. The understanding of changes in concrete properties due to variations in curing conditions from climate change is an imminent task that has to be resolved. Among the durability properties of concrete, freezing-and-thawing (FT) resistance is most directly affected by climate change. However, in all the studies conducted on the FT behavior of concrete, the dramatic changes in environmental conditions due to climate change were not considered. Therefore, the focus of this study is to understand the FT performance of concrete under extreme changes in temperature and relative humidity (RH) during curing. To find the relationship between the changes in curing conditions and FT resistance levels as a function of time, a three-dimensional (3-D) satisfaction surface graph was developed using the Bayesian probabilistic method. Then, an example of 3-D satisfaction surface diagrams for FT resistance based on the weather conditions in New York City between 2001 and 2100 was shown. Furthermore, considering the reduction rate of the average annual FT cycle due to climate change, this study confirmed that FT resistance performance increased. This approach contributes to a performance-based evaluation (PBE) strategy for concrete exposed to FT cycles under various environmental conditions. The study details and results are discussed in the paper.

Keywords: climate change; freezing-and-thawing (FT) resistance life; performance-based evaluation (PBE).

INTRODUCTION

The world has achieved industrialization using fossil fuels as an energy source. The use of fossil fuels emits greenhouse gases, which destroy the ozone layer. The destruction of the ozone layer has caused severe climate change in the twenty-first century due to global warming, resulting in phenomena such as heavily localized rainfall, snowfall, and typhoons. These abnormal weather patterns have induced critical global challenges that the world is facing presently.[1-3]

According to the Intergovernmental Panel on Climate Change (IPCC) Sixth Assessment Report (AR6), published in 2021, global warming has increased the average temperature of the Earth's surface by 1.09°C over the period of 1980 to 2020 (range between 0.95 and 1.20°C). The projected climate change is expected to have detrimental impacts on the environment and ecology, which will lead to economic and social challenges.[4]

Following this historical footstep, the cement and concrete industries have suffered from carbon emission reduction policies such as the net-zero policy. In addition, design and construction regulations have been strengthened to combat performance degradation that can occur during the casting and curing processes due to climate change. Therefore, it is important to understand the effect of temperature and relative humidity (RH) on the casting and curing processes of concrete used in construction projects. Changes in temperature and RH affect the moisture behavior within the concrete, leading to a reduction in entrained air content, slump, and hydration, which can lead to multiple cracking and internal pore formations that deteriorate the durability of concrete.[5-8]

Concrete durability performance is sensitive to changes in curing temperature and RH, which can significantly affect its freezing-and-thawing (FT) resistance. FT causes the free water inside the concrete to freeze, leading to volumetric expansion and ultimately leading to crack formations. Repeated FT leads to concrete quality degradation and durability degradation.[9] Additionally, during the curing process, concrete is particularly vulnerable to changes in temperature and RH. If the external temperature decreases and RH increases rapidly, the moisture inside the concrete may freeze prior to being fully hardened. Through repeated FT cycles, water can easily freeze and expand, potentially causing premature freeze damage.[10,11] Prolonged FT cycles can degrade the durability of concrete, thus causing serviceability problems in the structures.[12,13] Therefore, measures to overcome the abnormal deviations in the conditions in handling, mixing, transporting, and curing of concrete are required.[14-17]

In this study, the characteristics of concrete with severe fluctuations in curing conditions, namely temperature and RH, due to climate change, are studied. More specifically, concrete specimens were prepared according to ASTM C192/C192M-12[18] and cured under various temperature and RH conditions to understand the change in concrete properties. FT tests were conducted to measure the relative dynamic modulus of elasticity (RDME) after 100, 200, and 300 cycles according to ASTM C666/C666M-15.[17,19]

It is nearly impossible to evaluate the FT resistance life of concrete by only conducting tests due to changes in curing conditions of temperature and RH because the sufficient number of specimens that reflect all the changes occurring over 100 years is too large to consider. Therefore,

ACI Materials Journal, V. 123, No. 2, March 2026.
MS No. M-2025-062.R2, doi: 10.14359/51749445, received August 12, 2025, and reviewed under Institute publication policies. Pertinent discussion including author's closure, if any, will be published ten months from this journal's date if the discussion is received within four months of the paper's print publication.

Table 1—Mixture proportions of concrete

Maximum coarse aggregate size, mm	Slump, mm	w/b, %	Percentage of fine aggregate (s/a), %	Air, %	kg/m^3 Water (W)	Cement (C)	Fine aggregate (S)	Coarse aggregate (G)	f_{ck}, MPa
25	120.0	55.0	42.0	5.0	183.4	333.4	677.3	1013.0	27

Note: f_{ck} is design compressive strength.

to investigate the climate change-altered FT behavior in concrete, probabilistic statistical methods should be used to identify trends that affect performance. The representative method using such probabilistic statistics is performance-based evaluation (PBE). The PBE method uses Bayesian probabilistic statistics to determine the satisfaction level of a target structure, where the x-, y-, and z-axes represent the FT resistance life, the curing condition, and the satisfaction level, respectively. An example of three-dimensional (3-D) satisfaction diagrams for FT resistance life of a target concrete structure located in New York City is shown. Additionally, to reflect the annual FT cycles due to climate change, the study results of the annual FT cycles obtained from the Federal Highway Administration (FHWA) report and the United States Environmental Protection Agency (U.S. EPA) reports[20,21] were used for the PBE of FT resistance life. The FT cycles over 100 years decreased from 5400 to 3519 cycles, which was induced by changes in the temperature and RH curing condition ranges: 35 to 40°C and 65 to 90%, respectively. Using these changes in temperature, RH, and FT cycles, the effect on FT resistance life was reanalyzed for comparison purposes.

RESEARCH SIGNIFICANCE

This study proposes a method to evaluate the FT performance of concrete under various conditions by using Bayesian probability statistics to calculate the satisfaction curve (SC) for temperatures ranging from 8 to 45°C and RH levels ranging from 40 to 95%. The analysis results are presented as a 3-D satisfaction surface (SS) with a duration of 100 years to account for time dependency. Additionally, the FT resistance life was calculated considering the annual average FT cycles from the FHWA and the reduced annual average FT cycles projected by the U.S. EPA to account for climate change.

EXPERIMENTAL INVESTIGATION

Specimens

The mixture proportions used in this study are listed in Table 1. The water-binder ratio (w/b) was 55%, and only ordinary portland cement was used as the binder. The maximum size of the coarse aggregate was 25 mm, the slump was 120 mm, the fine aggregate ratio was 42%, the air content was 5%, and the 28-day compressive design strength was 27 MPa. Cylindrical concrete specimens (Φ100 x 200 mm) were prepared for compressive strength and FT tests in accordance with ASTM C192/C192M.[18] Five specimens were prepared for each test. To accurately represent the mean trend of the test results, the minimum and maximum values were excluded from the test data. Fresh concrete was cast in a laboratory environmental setting with a temperature of 23°C and RH of 65%. They were subsequently demolded 24 hours after casting. The curing conditions applied after demolding are described in the following section.

Curing condition

Concrete is typically cured under standard temperature and RH conditions of approximately 23 ± 2°C and 95% or higher, respectively. These conditions do not account for variations in climate. In this study, ordinary portland cement was used to produce normal-strength concrete for investigating the relationship between temperature and RH curing conditions and concrete strength. Temperature gradients within the specimens were assumed to be negligible due to their small size (Φ100 x 200 mm) and the use of curing chambers with constant temperature and RH for each temperature and RH combination curing conditions.

The annual and monthly average temperatures and RHs over the past 10 years in the New York metropolitan area were obtained from the weather survey website, as shown in Fig. 1. It illustrates that the most suitable period for concrete casting is between April and October, as evident from Fig. 1(b) and (d). The appropriate curing temperature and RH range were 15 to 30°C and 50 to 90%, respectively.

To account for the changes in temperature and RH due to climate change, low-temperature curing conditions of 15°C or less—namely, 8 and 12°C—were selected for the study. With respect to high-temperature curing conditions, temperatures of 30°C or higher—namely, 35, 40, and 45°C—were selected. RH was selected based on the monthly average of 65% from April to October, with the extreme RH condition set at 95% or higher, and the low RH condition set at 40% or lower.

Compressive strength test method

Concrete cylindrical specimens (Φ100 x 200 mm) were prepared according to ASTM C192/C192M.[18] Compressive strength of concrete is typically measured at 3, 7, and 28 days to evaluate early-, intermediate-, and standard-age strength according to ASTM C39/C39M-05,[22] respectively. The contact surfaces with the testing machine were ground flat, and rubber caps were used on the contact surfaces to prevent load eccentricity according to ASTM C1231/C1231M-09,[23] which permits the use of such caps provided that the rubber cap satisfies the specified hardness and thickness requirements. The specimen was applied with a load control rate of 0.6 ± 0.2 MPa/s. A universal testing machine with a maximum capacity of 1000 kN and an accuracy of 500 N was used for the test. All compressive strength tests were conducted after the specimens reached thermal equilibrium at room temperature. Therefore, eigen-stresses caused

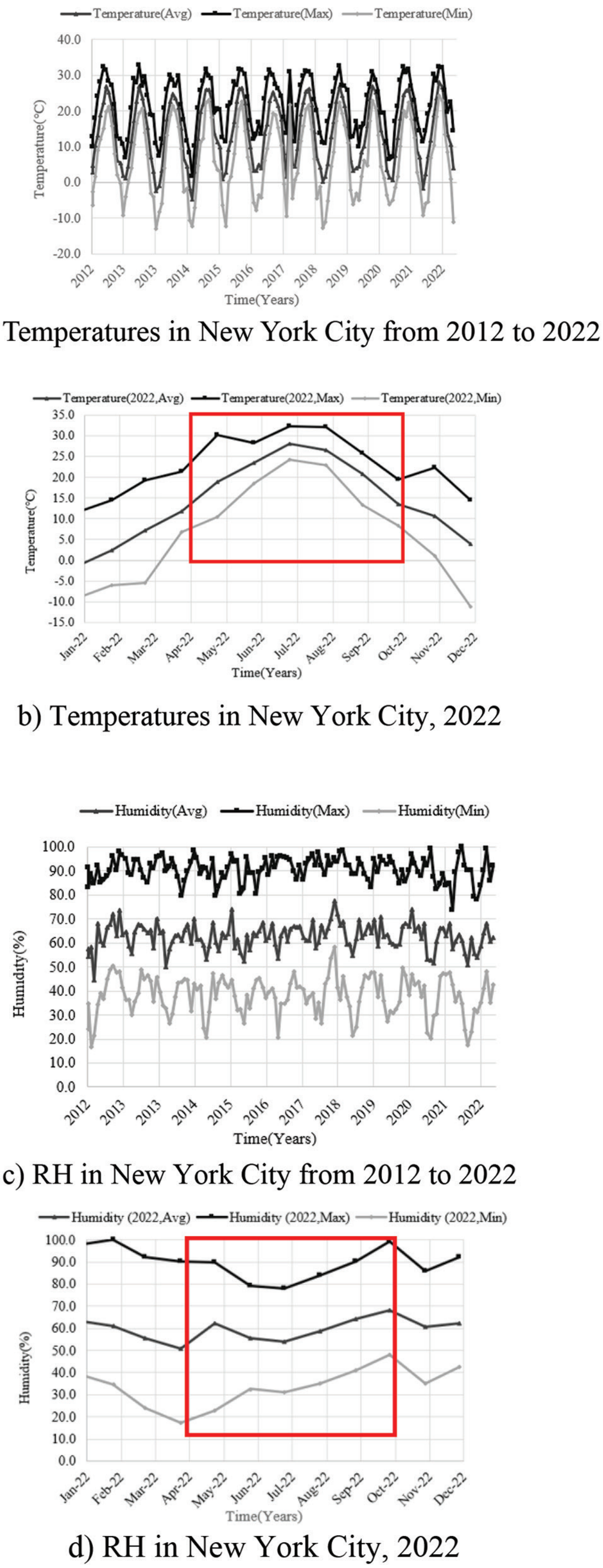

a) Temperatures in New York City from 2012 to 2022

b) Temperatures in New York City, 2022

c) RH in New York City from 2012 to 2022

d) RH in New York City, 2022

Fig. 1—New York City weather data for past 10 years, courtesy of U.S. Weather Underground.

by differences between the zero-stress reference temperature and the actual temperature were not considered.

Freezing-and-thawing test method

The FT tests were conducted in accordance with ASTM C666/C666M.[19] The central temperature of the concrete specimens was maintained at –18°C during freezing and +4°C during thawing in an FT chamber. Each FT cycle ensured that the maximum and minimum temperatures at the center of the specimen were within the range of 4 ± 2°C and –18 ± 2°C, respectively. More specifically, the temperature of the specimen should not fall below –20°C or rise above 6°C. The cycles consisted of 4 hours of freezing followed by 4 hours of thawing. The RDME of the specimen was obtained before and after 300 cycles, in accordance with ASTM C215-19.[24] Typically, FT tests are concluded after 300 cycles, but if the RDME drops below 60%, the test may be terminated instantly. In this study, measurements were taken at different cycles (0, 100, 200, and 300 cycles) under different curing conditions to calculate the RDME using Eq. (1) and Eq. (2)

$$P_c = \left(\frac{{n_c}^2}{{n_o}^2}\right) \times 100 \qquad (1)$$

where P_c is the RDME (%) after FT cycle N_o; n_c^2 is the primary resonance frequency (Hz) of deformation vibration in FT cycle N_o; and n_o^2 is the primary resonance frequency (Hz) of deformation vibration in FT cycle 0

$$DF = \frac{P_c N_o}{M} \qquad (2)$$

where DF is the durability index of the test specimen; P_c is the RDME (%) in cycle N_o; N_o is the number of cycles in which the RDME becomes 60% or the number of cycles at the end of the FT exposure; and M is the cycle at the end of the FT exposure.

ANALYTICAL INVESTIGATION

Performance-based evaluation method

Designing structures to satisfy design requirements, standards, and specifications based on structural types and use is called performance-based design (PBD). According to the International Council for Building Research report, approaching structures from a performance perspective means emphasizing results over methods or processes.[25] In general, prescriptive design methods, such as the limit state, working stress, and ultimate strength design methods, use resistance coefficients by calculating stiffness and load-carrying capacity. These methods tend to be driven by satisfying design requirements of common goals and specifications. More specifically, the *fib* Model Code adopts a deemed-to-satisfy approach for FT deterioration, which assumes a service life of 50 or 100 years, provided that the concrete satisfies the minimum requirements for compressive strength, air content, water-cement ratio (*w*/*c*), cement content, and cover thickness according to the designated exposure grade or limit states. However, these design criteria and specifications limit designers' ability to achieve design solutions with multiple options for various environmental conditions.

The PBE method used in this study evaluates the material performance satisfaction of concrete using new design solutions, interpretation methods, and test results for

Table 2—Compressive strength test results

Case	Compressive strength, MPa		
	3 days	7 days	28 days
T8H40	11.20 ± 0.25	16.19 ± 0.56	21.23 ± 0.38
T8H65	14.99 ± 0.46	18.25 ± 0.53	25.93 ± 1.56
T8H95	15.71 ± 0.55	20.30 ± 0.57	28.90 ± 0.61
T12H40	11.52 ± 0.33	16.56 ± 0.60	22.77 ± 0.55
T12H65	15.23 ± 0.79	21.35 ± 0.90	25.93 ± 0.84
T12H95	17.19 ± 0.36	24.52 ± 0.76	31.82 ± 0.93
T35H40	15.12 ± 1.47	19.34 ± 0.88	26.53 ± 0.25
T35H65	18.32 ± 1.59	23.83 ± 0.97	28.18 ± 1.13
T35H95	20.27 ± 0.11	25.70 ± 0.92	30.23 ± 2.09
T40H40	16.12 ± 2.78	19.34 ± 1.30	24.01 ± 0.32
T40H65	18.32 ± 1.21	22.80 ± 1.04	27.62 ± 0.98
T40H95	18.27 ± 1.52	23.70 ± 0.31	28.19 ± 1.29
T45H40	18.35 ± 0.19	21.22 ± 1.02	25.81 ± 0.72
T45H65	18.69 ± 1.81	20.68 ± 0.46	25.57 ± 0.59
T45H95	19.26 ± 0.91	24.66 ± 1.54	28.83 ± 0.80

probabilistic statistical determination. A satisfaction diagram is created using the Bayesian probability method, which uses the information obtained from sampling data to evaluate the satisfaction probability. Specifically, the normal probability distribution function is used to generate virtual data to compensate for the insufficient number of available test data points, which can supplement the data points needed for the development of SCs.[24-27] Through this approach, PBDs that accommodate diverse requirements at construction sites can be developed.

The lognormal cumulative distribution method is used to determine the satisfaction probability. The method uses a probability function that requires three variables: material variable value, mean value, and standard deviation for calculation, as shown in Eq. (3). The Bayesian probabilistic method was used to create a fragility curve for seismic failure evaluation. In Eq. (3), the a_i value is the material variable, which is the result value of RDME according to the FT test results for the temperature and RH curing conditions, and the N value is the number of material variable data points.

In fragility analysis, 1 and 0 are assigned to a structure damaged or undamaged by an earthquake, respectively. In contrast, the PBE of the material performance property is assigned a value of 1 or 0 for satisfying or not satisfying the design requirement, respectively. If these three variable data are evaluated by the Bayesian probability method, the result would be in the form of an accrued curve of the assigned lognormal distribution. Then the average value and standard deviation are obtained to draw an SC[26-29]

$$L = \prod_{i=1}^{N}[F(a_i)]^{x_i}[1 - F(a_i)]^{1-x_i} \tag{3}$$

where $F(.)$ is the SC of a specific material requirement; a_i is the design material requirement of variable I; x_i is determined to be 0 or 1 depending on the satisfaction to the material performance value, such as a_i; and N is determined by the total number of related material data obtained for material performance evaluation.

Compressive strength results and discussion

The compressive strength was measured at 3, 7, and 28 days after concrete casting. For all temperature and RH combinations, three specimens were tested to obtain the average strengths. The denomination system for the concrete specimens is as follows: "T" represents the curing temperature (°C), and "H" denotes the curing RH (%). The test results are shown in Table 2 and Fig. 2. The results showed that, as the curing age increased from 3 to 28 days, the strengths increased for all curing conditions, as expected. As shown in Fig. 2(a) to (c), compressive strength generally increased as the curing temperature increased, with the highest compressive strength observed at a temperature of 35°C. However, at 40 and 45°C, the compressive strength slightly decreased due to the effects of high temperature, showing an irregular trend. For the 3-day strength results, the specimens cured at 8 and 12°C had lower strengths than those cured under 35, 40, and 45°C. More specifically, the 3-day strengths of 8 and 12°C with RH of 95% were 6 to 29% lower than the specimens cured under temperatures of 35, 40, and 45°C with RH of 95%. For 7-day strengths, the trend was similar to that of 3-day strengths. More specifically, the 7-day strengths of 8 and 12°C were 16 to 21% lower than the specimens cured under temperatures of 35, 40, and 45°C.

The 28-day strengths showed no clear trend. Meanwhile, for all temperature curing conditions with RH of 95%, the 28-day strengths satisfied the target strength of the mixture of 27 MPa. The specimens that satisfied the target strength of 27 MPa were T8H95, T12H95, T35H40, T35H65, T35H95, T40H65, T40H95, and T45H95. As shown in Fig. 2(d) to (h), the strength increased as RH increased. At temperatures of

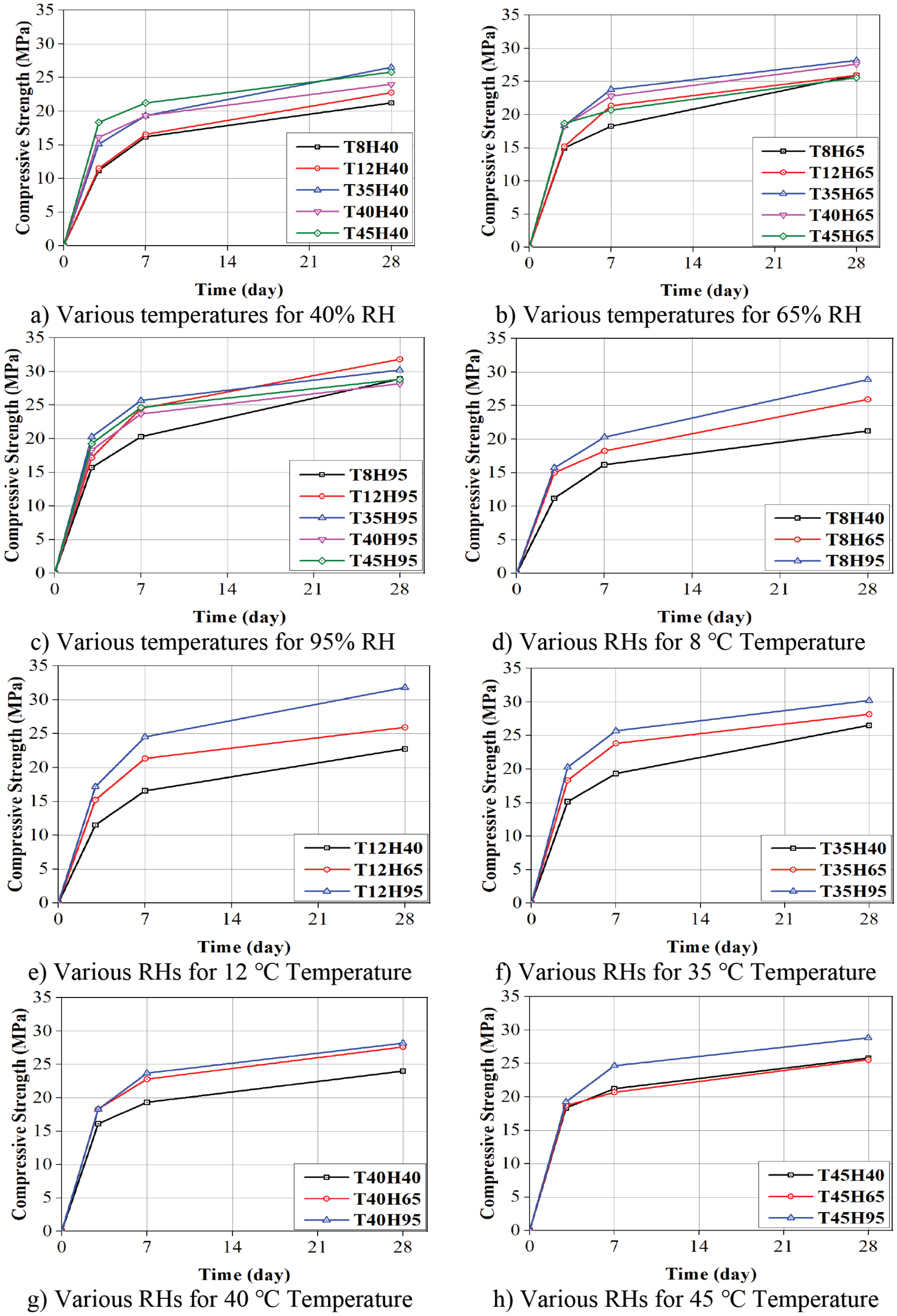

Fig. 2—Compressive strength results for various temperatures and RH curing conditions.

8 and 12°C, the effect of RH on the strength increase was significant. However, the effect was minimal at temperatures of 35, 40, and 45°C. More specifically, when the RH increased from 40 to 95%, the 28-day strength increased by 40% at 12°C and by 12% at 45°C, respectively. The trend can be attributed to a high RH condition providing enough moisture for the hydration reaction. In the case of a curing temperature of 45°C, the number of pores and microcracks increased inside the concrete due to the nonuniform diffusion of hydration products and differences in the thermal expansion coefficients of concrete materials, resulting in an unexpected trend in compressive strength.[30,31] The specimens cured under relatively extreme conditions of 35 to 40°C and RH of 65 to 95% satisfied the target strength requirement of 27 MPa.

Freezing-and-thawing test results and discussion

The FT test was conducted in accordance with ASTM C666/C666M. For all temperature and RH curing condition combinations, three specimens were tested to obtain the average RDME. The test results are shown in Table 3 and Fig. 3. The RDME of specimens was measured after 100, 200, and 300 FT cycles. The result showed that, as the FT increased from 100 to 300 cycles, the RDME decreased for all curing conditions, as expected. As shown in

Table 3—FT test results

	RDME, %			
Case	0 cycles, %	100 cycles, %	200 cycles, %	300 cycles, %
T8H40	100.00	84.67 ± 0.45	73.60 ± 1.06	69.13 ± 1.04
T8H65	100.00	84.36 ± 0.95	73.10 ± 0.79	66.70 ± 1.73
T8H95	100.00	86.13 ± 1.23	71.60 ± 1.06	65.03 ± 1.42
T12H40	100.00	89.43 ± 1.84	76.46 ± 1.17	69.60 ± 1.45
T12H65	100.00	88.76 ± 0.40	76.83 ± 1.61	69.03 ± 1.17
T12H95	100.00	87.76 ± 2.03	74.00 ± 0.75	67.60 ± 0.30
T35H40	100.00	92.03 ± 1.86	85.06 ± 2.14	77.50 ± 3.64
T35H65	100.00	94.00 ± 1.05	85.63 ± 1.07	75.23 ± 1.95
T35H95	100.00	95.36 ± 0.85	90.60 ± 0.85	85.46 ± 1.11
T40H40	100.00	91.90 ± 1.85	83.40 ± 2.03	77.63 ± 2.46
T40H65	100.00	93.03 ± 2.40	83.86 ± 1.66	74.60 ± 2.21
T40H95	100.00	92.49 ± 1.13	86.69 ± 0.35	83.30 ± 0.91
T45H40	100.00	93.30 ± 1.44	83.20 ± 1.49	69.06 ± 1.80
T45H65	100.00	90.26 ± 2.67	81.56 ± 1.18	68.33 ± 0.75
T45H95	100.00	93.76 ± 2.93	80.03 ± 2.21	72.33 ± 2.06

Fig. 3(a) to (c), the RDME generally increased as the curing temperature increased, with the highest RDME observed at a temperature of 35°C. However, at 40 and 45°C, the RDME slightly decreased due to the effects of high temperature, similar to the trend in compressive strength results. For 100 cycles, the specimens cured at 8 and 12°C had lower RDME than those cured at 35, 40, and 45°C. More specifically, for the specimens cured at 8 and 12°C and 95% RH, the RDMEs after 100 FT cycles were 3 to 10% lower than those for the specimens cured at 35, 40, and 45°C and RH of 95%. For the 200-cycle results, the trend was similar to the 100-cycle results. More specifically, the RDME results of 8 and 12°C and 95% RH after 200 cycles were 6 to 26% lower than those from the specimens cured at 35, 40, and 45°C and 95% RH. For the 300-cycle results, the RDME results showed that they increased with increasing temperature at 95% RH. However, no clear trend can be observed in the results from the specimens cured under other RH conditions. More specifically, the 300-cycle RDME results from the specimens cured at 8 and 12°C were 8 to 31% lower than those from the specimens cured at 35 and 40°C. In the case of a curing temperature of 45°C, similar to the trend in compressive strength results, RDMEs decreased due to the formation of microcracks.[31]

In all curing conditions, the 300-cycle RDMEs satisfied the criterion of requiring greater than 60% of the RDME of the specimens without FT cycles, as specified in ASTM C666/C666M.[19] If the RDME requirement increases to 70%, the specimens cured at 35°C or higher can satisfy the requirement. In fact, the T35H95 and T40H95 specimens can satisfy the requirement even if the requirement is increased to 80%. Under low-temperature curing conditions, RDME decreases as RH increases. In contrast, under high-temperature curing conditions, RDME increases with an increase in RH. As shown in Fig. 3(d) and (e), for the low-temperature curing condition, RDME decreased by 3 to 6% as RH increased. The result trend can be attributed to hydration reactions being delayed due to the reduction in internal free water from the low-temperature condition of FT cycles. On the other hand, as shown in Fig. 3(g) and (h), for the high-temperature curing condition, RDME increased by 5 to 10% as curing RH increased. High-temperature curing conditions induce internal moisture movement, promoting greater hydration reactions and an increase in RDME. As FT cycles increased, the RDME reduction rate was approximately 10 to 15% for the specimens cured at 35 and 40°C, while the RDME increase rate was the highest as RH increased under the same temperature conditions. Therefore, the optimal curing condition was identified as a temperature of 35°C and an RH of 95%.

ANALYTICAL RESULTS AND DISCUSSION

Freezing-and-thawing resistance life evaluation considering climate change in New York City

Climate change is decreasing the average number of FT cycles occurring in a season due to gradually increasing temperatures. To predict the FT resistance life of a concrete structure, it is necessary to estimate the average FT cycle reduction in the region where the structure is located. For this study, the target location to consider climate change conditions was selected as New York City. According to the FHWA report,[20] the annual FT cycles occurring in and around New York City are approximately 54 cycles per year. Therefore, the FT cycles occurring in New York City over 1 to 100 years would be 54 to 5400 cycles. According to the U.S. EPA report,[21] the annual FT reduction was 0.38 days, as shown in Fig. 4. Applying this reduction as a base to incorporate the effect of climate change, the FT cycles occurring in New York City over 1 to 100 years would be 54 to 3519 cycles.

To evaluate the FT resistance life of a concrete structure in New York City, the prediction of RDME as a function of the

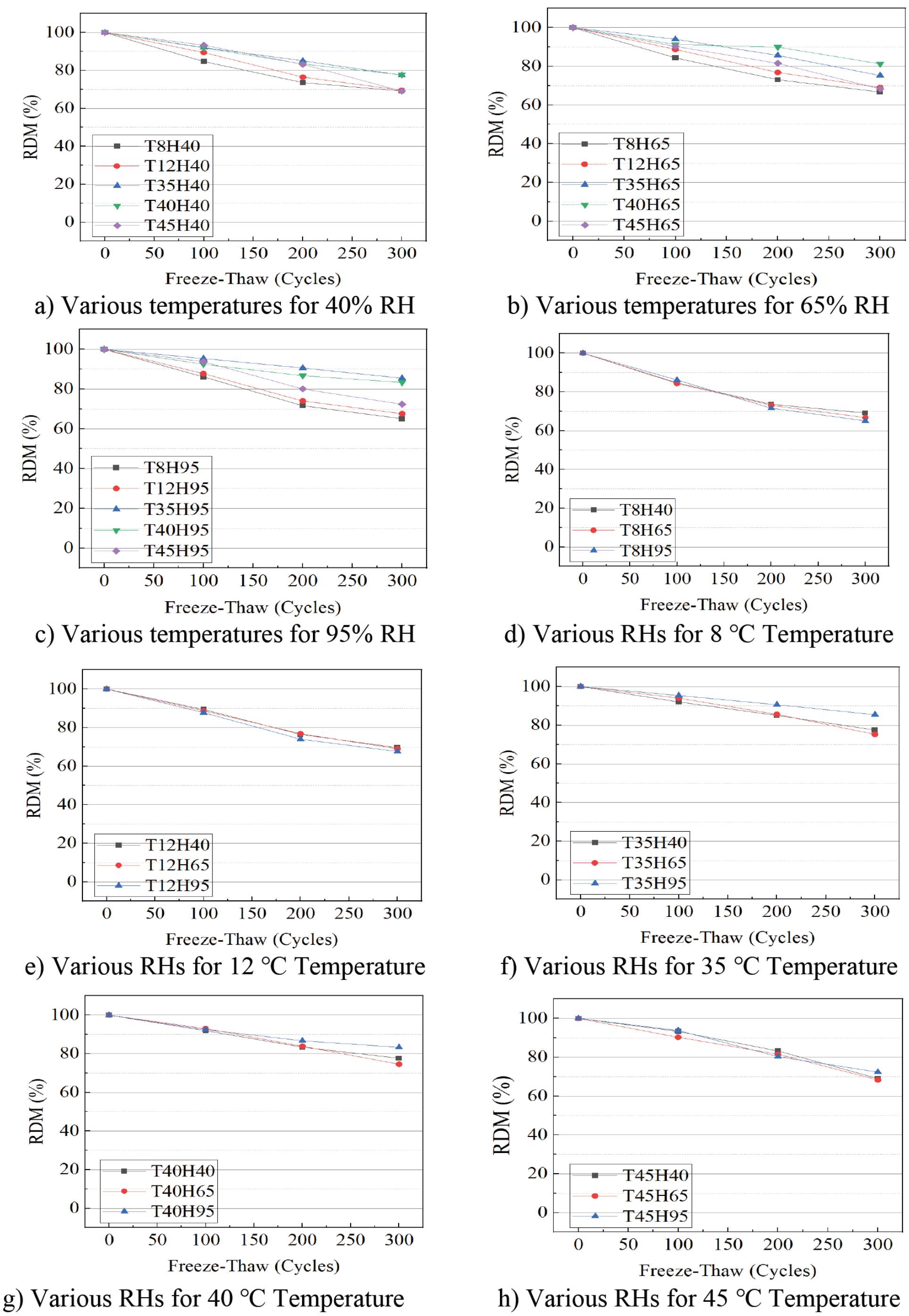

Fig. 3—RDME results after 300 FT cycles cured under various temperatures and RHs.

number of FT cycles occurring annually is needed. Using the predicted RDMEs, the FT resistance of the concrete structure during its service life can be obtained through drawing satisfaction graphs. However, it is nearly impossible to obtain an RDME equation for an extended duration, such as 100 or 150 years, due to the time and cost required to perform FT cycle tests. Also, the RDME equations for various combinations of temperature and RH curing conditions are nearly impossible to obtain due to an insurmountable amount of work required to obtain a sufficient number of FT RDME data. Therefore, based on the RDME data obtained from the FT tests with a limited number of FT cycles in this study, the RDME equations were obtained for the curing conditions applied in this study. The base equation that was used to curve-fit the data was as follows

$$\text{RDME} = c_1 \times \ln(N_{FT}) + c_2 \quad (4)$$

where RDME is the relative dynamic modulus of elasticity; c_1 and c_2 are the coefficients obtained from the curve fitting; and N_{FT} is the number of FT cycles.

All the curve-fitted equations for the curing conditions considered in this study are shown in Table 4. The equations are derived based on the criterion of RDME equaling 60% of the RDME without FT damage. More specifically, for each curing condition, data-fitted equations were proposed

Table 4—Number of years when RDME falls below 60%

Case	RDME prediction formula	Coefficient of determination	Failure years		Failure cycles
		R^2	FHWA standard	U.S. EPA standard	
T8H40	RDME = –14.34ln(N) + 150.41	0.99	11	11	549
T8H65	RDME = –16.09ln(N) + 158.44	0.99	9	9	455
T8H95	RDME = –19.4ln(N) + 175.16	0.99	8	8	379
T12H40	RDME = –18.12ln(N) + 172.77	0.99	10	10	505
T12H65	RDME = –17.88ln(N) + 171.22	0.99	10	10	504
T12H95	RDME = –18.51ln(N) + 172.76	0.99	9	9	443
T35H40	RDME = –12.88ln(N) + 151.89	0.97	23	25	1259
T35H65	RDME = –16.55ln(N) + 171.03	0.96	15	17	822
T35H95	RDME = –8.78ln(N) + 136.15	0.97	108	None	5877
T40H40	RDME = –12.91ln(N) + 151.48	0.99	22	25	1199
T40H65	RDME = –16.39ln(N) + 169.12	0.98	10	10	519
T40H95	RDME = –8.37ln(N) + 131.03	0.99	89	None	4876
T45H40	RDME = –18.6ln(N) + 179.72	0.94	10	10	508
T45H65	RDME = –19.16ln(N) + 179.75	0.93	10	10	519
T45H95	RDME = –22.19ln(N) + 196.42	0.99	11	11	562

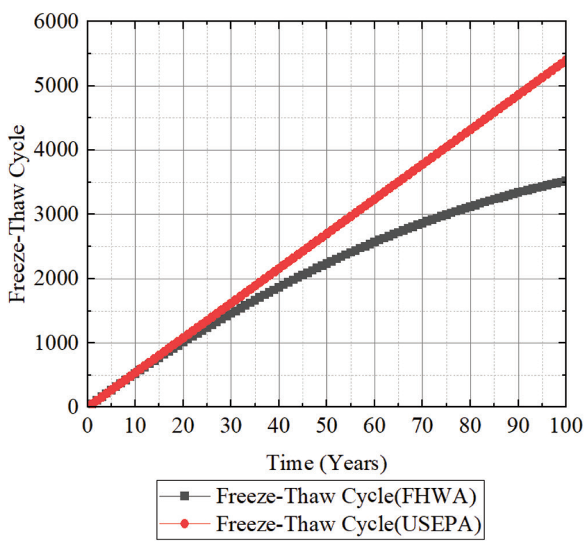

Fig. 4—Changes in FT cycle due to climate change.

to represent the relationship between RDME and 100, 200, and 300 FT cycles. It should be noted that the fitted RDME model (Eq. (4)) is extrapolated beyond 300 FT cycles to estimate the long-term FT resistance life. This extrapolation is based on the assumption that the RDME degradation trend observed up to 300 cycles continues in a similar pattern. The logarithmic nature of the model reflects the decelerating damage accumulation typically observed in concrete under FT conditions, as reported by Chen and Qiao[32] and Yan et al.[33] While this approach introduces uncertainty, it provides a rational basis for performance comparison under various temperature and RH combinations during curing. Table 4 also shows the number of years to reach the 60% RDME using both the FHWA and U.S. EPA standards. It should also be noted that the model does not explicitly consider strength development due to aging beyond 28 days. At this stage, additional strength development has minimal influence on FT resistance, as FT resistance is more critically influenced by internal pore structure and external exposure conditions.[13]

With respect to the FT resistance life prediction, the T8H95 specimen had the shortest FT resistance life of 9 years, whereas the T35H95 specimen had the longest FT resistance life of 108 years. Similar to the previous FT test results, the FT resistance life of specimens cured at lower temperatures of 8 and 12°C was two to 13 times shorter than that of specimens cured at higher temperatures of 35, 40, and 45°C. For 8 and 12°C curing temperatures, the FT resistance life decreased by 10 to 20% from increasing RH, whereas for 35 and 40°C curing temperatures, the FT resistance life increased four to five times from increasing RH. This indicates that the FT resistance life of concrete is directly influenced by the curing conditions, including temperature and RH.

Performance-based evaluation development of freezing-and-thawing resistance life

To develop FT SCs, the yearly RDME is needed to predict the state of FT resistance of the concrete structure. In this study, the yearly RDME considering curing conditions was obtained from the curve-fitted RDME equations as a function of the number of FT cycles, shown in Table 4. The FT SCs were developed based on two parameters: temperature and RH curing conditions. The criterion used to determine the success/failure of the satisfaction was 60% RDME for a duration of 1 to 100 years. Using the Bayesian probabilistic method, the satisfaction graphs can be developed by considering the annual FT cycles proposed by the FHWA standard, as shown in Fig. 5. The two-dimensional (2-D) SCs are shown in Fig. 5(a) and (b), and the 3-D SSs are shown in Fig. 5(c) and (d). The difference between the 2-D and 3-D graphs comes from the time dependency of the durability performance of concrete. For example, the 2-D FT SC is drawn at a selected time of concrete life, such as the

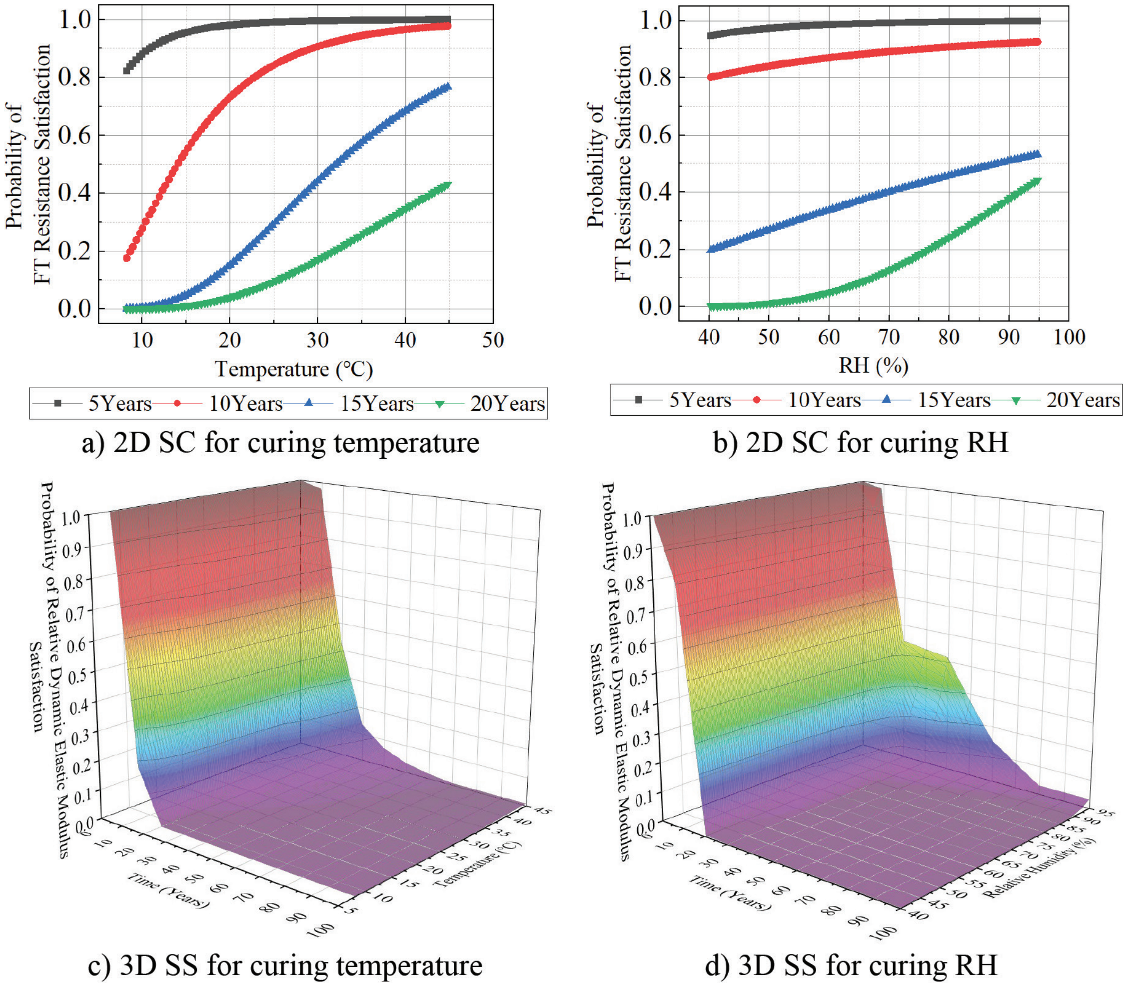

a) 2D SC for curing temperature
b) 2D SC for curing RH
c) 3D SS for curing temperature
d) 3D SS for curing RH

Fig. 5—FHWA FT resistance life satisfaction graphs according to temperature and RH.

first, 20th, or 100th year. However, the 3-D FT SS is drawn for a duration of 100 years of service life. More specifically, 100 2-D SCs would be used to draw a 3-D SS.

As shown in Fig. 5(a), the satisfaction level decreased as the FT exposure time increased, as expected. As shown in Fig. 5(a), the satisfaction increase rate after 5 years of FT exposure was relatively similar for all the curing temperatures, while the satisfaction increase rate after 10, 15, and 20 years of FT exposure was significant as the curing temperature increased. For the 10-year FT resistance SC, the satisfaction percentage rapidly increased with curing temperature up to 20°C, then tapered off beyond 20°C. For 15- and 20-year FT resistance SCs, the satisfaction percentage increase is more gradual as the curing temperature increases.

The trend in RH results is similar to the temperature results, as shown in Fig. 5(b). As shown in Fig. 5(b), the satisfaction level decreased as the FT exposure time increased, as expected. Unlike the temperature results, the RH results show that the increase rate for all FT exposure durations (that is, 5, 10, 15, and 20 years) is more gradual as the RH increases. For the 5-, 10-, and 15-year FT exposures, the satisfaction results show almost linear relationships. Only for the 20-year FT exposure, the satisfaction level for the specimens cured at 50% RH is 0%, but it gradually increases beyond the RH. The overall results showed that high satisfaction levels are shown for the 5- and 10-year FT exposures, and relatively low satisfaction levels are shown for the 15- and 20-year FT exposures. The 3-D FT resistance SSs developed for a duration of 100 years are shown in Fig. 5(c) and (d). The comparison of the FT resistance life predictions from the developed satisfaction graphs and the test data curve-fitted RDME equations reveals that the FT resistance life sharply decreased by 9 to 11 years for the temperature conditions of 8 and 12°C and the RH conditions of 40 and 65%. The reasonable comparison results indicate that the 3-D graph generated through PBE is reliable for use in evaluations of real scenarios.

As an example of PBE, a scenario is examined in which a structure is required to achieve a satisfaction level of 0.5 or higher and a target FT resistance life of at least 15 years. As shown in Fig. 5(a), this performance could be achieved at curing temperatures of 33°C or higher. As shown in Fig. 5(b), the RH should be maintained at 86% or higher. In addition, a structure cured at a temperature of 30°C and an RH of 90% is estimated to have an FT resistance life of approximately 14 years. To overcome the limited number of test data points in this study, supplemental data points generated from the normal probability distribution function were obtained. These generated virtual data points are used to generalize the evaluation results. The proposed method is based on a probabilistic framework designed to demonstrate

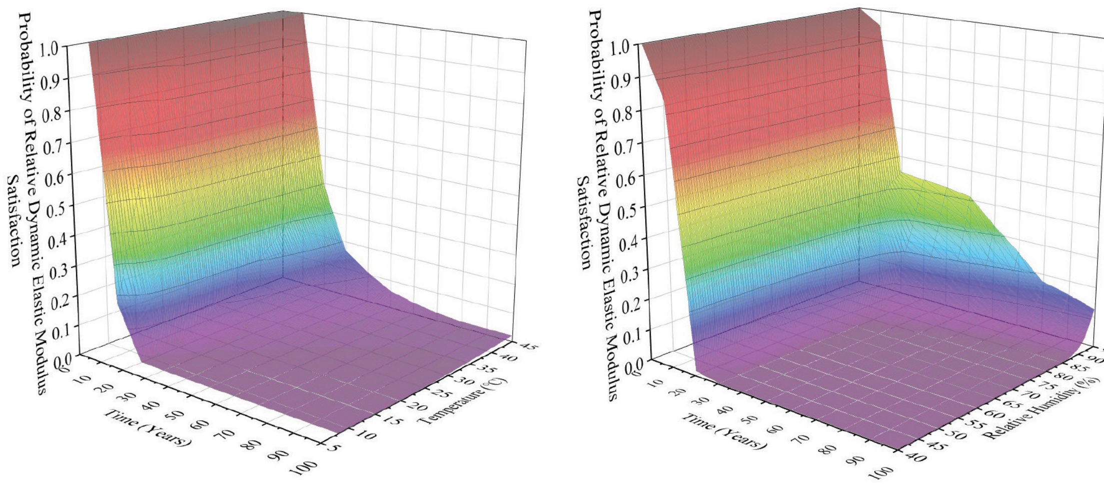

a) 3D SS for curing temperature

b) 3D SS for curing RH

Fig. 6—U.S. EPA FT resistance life satisfaction graphs according to temperature and RH.

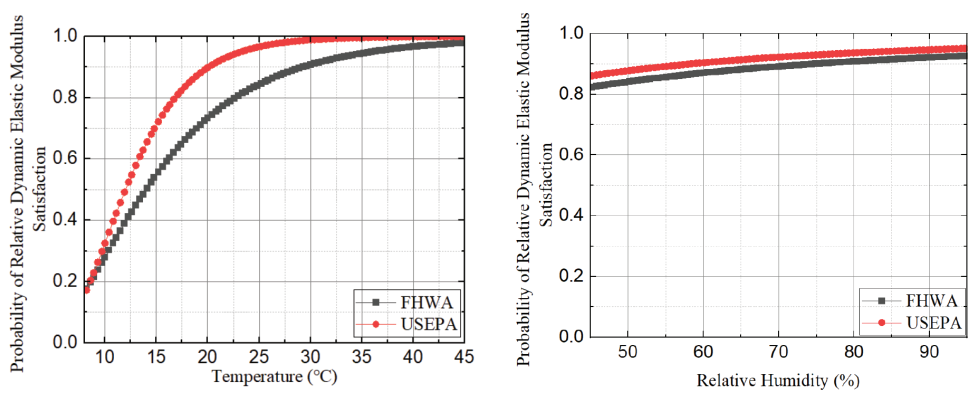

a) 2D SC for curing temperature

b) 2D SC for curing RH

Fig. 7—Comparison of 10-year FT resistance SCs for FHWA and U.S. EPA.

the applicability of PBE to FT resistance under various curing conditions. For further analysis, additional experimental investigations on aged or deteriorated concrete structures will be necessary in the future.

Freezing-and-thawing performance-based evaluation considering climate change in New York City

To develop the SC considering climate change in the New York City area, the FT cycle reduction rate of the U.S. EPA, shown in Fig. 6, was used. The U.S. EPA SSs for curing temperature and RH are shown in Fig. 6(a) and (b), respectively. Comparisons of the 10-year FT resistance SCs for curing temperature and RH developed based on climate change predictions of the FHWA and U.S. EPA are shown in Fig. 7(a) and (b), respectively. In general, FT resistance life increases when climate change is considered, because the annual FT cycles are reduced due to global warming. More specifically, the FT resistance life based on the FHWA climate change prediction increases after 10 years. The T35H40, T35H65, T40H40, and T45H95 specimens showed 2 to 3 years longer FT resistance life. On the other hand, the FT resistance life for the T35H95 and T40H95 specimens could not be calculated, because for the duration of 150 years, the reduction in annual FT days exceeded the annual FT cycles, which theoretically eliminated the possibility of an FT event occurring. Moreover, no changes in FT resistance life were observed under other temperature and RH curing combinations.

The 10-year FT resistance life SCs for curing temperature, developed based on the FHWA and U.S. EPA climate change predictions, showed the largest difference, as shown in Fig. 7. As shown in Fig. 7(a), the FT resistance life showed a difference of approximately 25% satisfaction percentage within the temperature range of 13 to 25°C when climate change was considered. With respect to the FT resistance life for curing RH, approximately a 10% difference in satisfaction percentage occurred, as shown in Fig. 7(b). This trend can be attributed to the annual FT cycles decreasing by 0.38 days due to U.S. EPA climate change predictions, leading to an increase in FT resistance life and satisfaction percentage.

Additionally, because the number of FT cycles decreases each year due to global warming, the 100-year FT satisfaction percentage calculations are conducted to consider the long-term climate change predictions from various organizations, such as the FHWA and U.S. EPA. The comparative analysis revealed that the duration required to reach the 50% FT resistance satisfaction percentage is over 16 years, which is the same for both the FHWA and U.S. EPA predictions.

However, the duration required to reach the 30% satisfaction percentage for temperature curing conditions differed, with the FHWA prediction giving 22 years and the U.S. EPA prediction giving 24 years. For RH curing conditions, the FHWA predicted 48 years, and the U.S. EPA predicted 63 years. These differences can be attributed to the increase in temperature due to the global warming phenomenon from climate change, leading to reduced FT cycles and increased FT satisfaction levels.

CONCLUSIONS

Based on the results of the study, the following conclusions are drawn:

1. In the freezing-and-thawing (FT) resistance tests under specific temperature and relative humidity (RH) curing conditions, relative dynamic modulus of elasticity (RDME) results from the specimens cured at 8 and 12°C were 8 to 31% lower than those from the specimens cured at 35 and 40°C. For the low-temperature curing condition, RDME decreased by 3 to 6% as RH increased, while for the high-temperature curing condition, RDME increased by 5 to 10% as RH increased.

2. Regarding the FT resistance prediction for New York City, the FT resistance lives of specimens cured at 8 and 12°C (considered as low curing temperatures) were two to 13 times shorter than those of specimens cured at 35, 40, and 45°C. At low temperatures of 8 and 12°C, the FT resistance life decreased by 10 to 20% as the RH curing condition increased. Conversely, at optimal temperatures of 35 and 40°C, the FT resistance life increased by four to five times as the RH curing condition increased.

3. The satisfaction increase rate after 5 years of FT exposure was relatively similar for all the curing temperatures, while the satisfaction increase rate after 10, 15, and 20 years of FT exposure was significant as the curing temperature increased. For 10-year FT resistance SC, the satisfaction percentage rapidly increased for the curing temperature up to 20°C, then tapered off beyond 20°C. The comparison of the FT resistance life predictions from the developed satisfaction graphs and the test data curve-fitted RDME equations revealed that the FT resistance life sharply decreased by 9 to 11 years for the temperature conditions of 8 and 12°C and the RH conditions of 40 and 65%.

4. The 10-year FT resistance life satisfaction curves (SCs) for curing temperature developed based on the Federal Highway Administration (FHWA) and United States Environmental Protection Agency (U.S. EPA) climate change predictions showed the largest difference. The FT resistance life showed a difference of approximately 25% satisfaction percentage within the temperature range of 13 to 25°C when climate change was considered. With respect to the FT resistance life for curing RH, approximately a 10% difference in satisfaction percentage occurred.

5. The proposed method offers a probabilistic framework for evaluating FT resistance based on satisfaction levels under various curing conditions, rather than relying on prescriptive life predictions. While the extrapolated RDME models provide useful insights into long-term performance, they are primarily intended for comparative purposes and require further validation. This study tried to overcome the limitations of test variability and curve fitting by performing the analysis using statistical averaging. This approach can be considered a performance-based evaluation (PBE) strategy for concrete exposed to FT cycles under various environmental conditions.

FURTHER STUDY

Because the study has already been completed, FT data of other cement type mixture proportions are not available at this time. Therefore, in a future study, more quantitative data from additional mixture proportions using various cement types, fly ash, silica fume, ground-granulated blast-furnace slag, and ferro-nickel slag will be collected. In addition, the durability behavior with respect to chloride penetration resistance and carbonation tests will be quantified.

AUTHOR BIOS

Jin-Su Kim *is a PhD Student in the Department of Civil and Environmental Engineering at Yonsei University, Sinchon, Seoul, South Korea. He received his BS from Induk University, Seoul, South Korea. His research interests include the durability of reinforced concrete structures in climatic environments.*

Woo-Ri Kwon *is an MS Student in the Department of Civil and Environmental Engineering at Yonsei University. She received her BS from Hanyang University's ERICA Campus, Ansan, Gyeonggi, South Korea. Her research interests include enhancing the durability of concrete with carbon fiber-reinforced polymer.*

Norhazilan Md Noor *is a Professor of structure and materials at Universiti Teknologi Malaysia, Skudai, Johor, Malaysia. He received his BS and MS from Universiti Teknologi Malaysia, and his PhD from Heriot-Watt University, Edinburgh, UK. His research interests include structural reliability and risk assessment, and probabilistic assessment and artificial intelligence (AI)-driven digital twin technologies for marine and oil and gas infrastructure.*

Jang-Ho Jay Kim *is a Professor of civil engineering and environmental engineering at Yonsei University. He received his BS from the University of California, Los Angeles, Los Angeles, CA; his MS from the University of California, Berkeley, Berkeley, CA; and his PhD from Northwestern University, Evanston, IL. His research interests include the performance-based evaluation of the durability of reinforced concrete structures.*

ACKNOWLEDGMENTS

This work is supported by the Korea Agency for Infrastructure Technology Advancement (KAIA) grant funded by the Ministry of Land, Infrastructure and Transport (Grant RS-2021-KA163381).

NOTATION

a_i = design material requirement of variable I
c_1, c_2 = coefficients obtained from curve fitting
DF = durability index of test specimen
$F(.)$ = SC of specific material requirement
M = cycle at end of FT exposure
N = determined by total number of related material data obtained for material performance evaluation
N_{FT} = number of FT cycles
N_o = number of cycles in which relative dynamic modulus of elasticity becomes 60% or number of cycles at end of freezing-and-thawing exposure
n_c^2 = primary resonance frequency (Hz) of deformation vibration in FT cycle N_o
n_o^2 = primary resonance frequency (Hz) of deformation vibration in FT cycle 0
P_c = relative dynamic modulus of elasticity (%) after freezing-and-thawing cycle N_o
x_i = determined to be 0 or 1 depending on satisfaction to material performance value such as a_i

REFERENCES

1. Anderson, K., "What was the Industrial Revolution's Environmental Impact?" Greenly Leaf Media, Aug. 25, 2024, https://greenly.earth/en-us/blog/ecology-news/what-was-the-industrial-revolutions-environmental-impact. (last accessed Feb. 23, 2026)

2. Neale, P. J.; Hylander, S.; Banaszak, A. T.; Häder, D.-P.; Rose, K. C.; Vione, D.; Wängberg, S.-Å.; Jansen, M. A. K.; Busquets, R.; Andersen, M. P. S.; Madronich, S.; Hanson, M. L.; Schikowski, T.; Solomon, K. R.; Sulzberger, B.; Wallington, T. J.; Heikkilä, A. M.; Pandey, K. K.; Andrady, A. L.; Bruckman, L. S.; White, C. C.; Zhu, L.; Bernhard, G. H.; Bais, A.; Aucamp, P. J.; Chiodo, G.; Cordero, R. R.; Petropavlovskikh, I.; Neale, R. E.; Olsen, C. M.; Hales, S.; Lal, A.; Lingham, G.; Rhodes, L. E.; Young, A. R.; Robson, T. M.; Robinson, S. A.; Barnes, P. W.; Bornman, J. F.; Harper, A. B.; Lee, H.; Mackenzie Calderón, R.; Ossola, R.; Paul, N. D.; Revell, L. E.; Wang, Q.-W.; and Zepp, R. G., "Environmental Consequences of Interacting Effects of Changes in Stratospheric Ozone, Ultraviolet Radiation, and Climate: UNEP Environmental Effects Assessment Panel, Update 2024," *Photochemical & Photobiological Sciences*, V. 24, No. 3, Mar. 2025, pp. 357-392.

3. Leal Filho, W.; Azul, A. M.; Brandli, L.; Lange Salvia, A.; and Wall, T., eds., *Affordable and Clean Energy*, Springer, Cham, Switzerland, 2021, 1309 pp.

4. IPCC Working Group 1 Technical Support Unit, eds., "Climate Change 2021: The Physical Science Basis," Working Group I Contribution to the Sixth Assessment Report of the Intergovernmental Panel on Climate Change, Cambridge University Press, Cambridge, UK, 2021, 2409 pp.

5. Shen, D., *Early-age Cracking Control on Modern Concrete*, Springer, Singapore, 2024, 439 pp.

6. Alshammari, T. O.; Guadagnini, M.; and Pilakoutas, K., "The Effect of Harsh Environmental Conditions on Concrete Plastic Shrinkage Cracks: Case Study Saudi Arabia," *Materials*, V. 15, No. 23, Dec. 2022, Article No. 8622. doi: 10.3390/ma15238622

7. Xia, D.; Yu, S.; Yu, J.; Feng, C.; Li, B.; Zheng, Z.; and Wu, H., "Damage Characteristics of Hybrid Fiber Reinforced Concrete Under the Freeze-Thaw Cycles and Compound-Salt Attack," *Case Studies in Construction Materials*, V. 18, July 2023, Article No. e01814. doi: 10.1016/j.cscm.2022.e01814

8. Fülöp, L.; Ferreira, M.; Bohner, E.; Valokoski, J.; Vuotari, J.; and Tirkkonen, T., "Inspection of Bridges for Effects of Air-Entrainment on the Porosity and Compressive Strength of Concretes," *Case Studies in Construction Materials*, V. 17, Dec. 2022, Article No. e01211. doi: 10.1016/j.cscm.2022.e01211

9. Ma, Q.; Xiao, J.; Ding, T.; Duan, Z.; Song, M.; and Cao, X., "The Prediction of Compressive Strength for Recycled Coarse Aggregate Concrete in Cold Region," *Case Studies in Construction Materials*, V. 19, Dec. 2023, Article No. e02546. doi: 10.1016/j.cscm.2023.e02546

10. Ji, Y., and Wang, D., "Durability of Recycled Aggregate Concrete in Cold Regions," *Case Studies in Construction Materials*, V. 17, Dec. 2022, Article No. e01475.

11. Guo, J.; Zhou, Z.; Zhang, Z.; Tang, J.; Li, X.; and Zou, Y., "Effects of Alternating Positive and Negative Temperature Curing on the Mechanical Properties of Ultra-High Performance Concrete," *Case Studies in Construction Materials*, V. 20, July 2024, Article No. e02752. doi: 10.1016/j.cscm.2023.e02752

12. Guo, J.; Sun, W.; Xu, Y.; Lin, W.; and Jing, W., "Damage Mechanism and Modeling of Concrete in Freeze–Thaw Cycles: A Review," *Buildings*, V. 12, No. 9, Sept. 2022, Article No. 1317. doi: 10.3390/buildings12091317

13. Luo, S.; Bai, T.; Guo, M.; Wei, Y.; and Ma, W., "Impact of Freeze–Thaw Cycles on the Long-Term Performance of Concrete Pavement and Related Improvement Measures: A Review," *Materials*, V. 15, No. 13, July 2022, Article No. 4568. doi: 10.3390/ma15134568

14. Wang, R.; Hu, Z.; Li, Y.; Wang, K.; and Zhang, H., "Review on the Deterioration and Approaches to Enhance the Durability of Concrete in the Freeze–Thaw Environment," *Construction and Building Materials*, V. 321, Feb. 2022, Article No. 126371. doi: 10.1016/j.conbuildmat.2022.126371

15. Joshaghani, A.; Balapour, M.; and Ramezanianpour, A. A., "Effect of Controlled Environmental Conditions on Mechanical, Microstructural and Durability Properties of Cement Mortar," *Construction and Building Materials*, V. 164, Mar. 2018, pp. 134-149. doi: 10.1016/j.conbuildmat.2017.12.206

16. Shen, X.; Li, L.; Cui, W.; and Feng, Y., "Coupled Heat and Moisture Transfer in Building Material with Freezing and Thawing Process," *Journal of Building Engineering*, V. 20, Nov. 2018, pp. 609-615. doi: 10.1016/j.jobe.2018.07.026

17. Chen, J.; Li, Y.; Li, Y.; Wen, L.; and Guo, H., "Effects of Curing Conditions with Different Temperature and Humidity on Damage Evolution of Concrete During Freeze–Thaw Cycling," *Materials and Structures*, V. 55, No. 2, Mar. 2022, Article No. 80. doi: 10.1617/s11527-022-01921-z

18. ASTM C192/C192M-12, "Standard Practice for Making and Curing Concrete Test Specimens in the Laboratory," ASTM International, West Conshohocken, PA, 2012, 8 pp.

19. ASTM C666/C666M-15, "Standard Test Method for Resistance of Concrete to Rapid Freezing and Thawing (Withdrawn 2024)," ASTM International, West Conshohocken, PA, 2015, 6 pp.

20. Hansen, W.; Jensen, E. A.; and Mohr, P., "The Effects of Higher Strength and Associated Concrete Properties on Pavement Performance," Report No. FHWA-RD-006-161, Federal Highway Administration, McLean, VA, 2001, 255 pp.

21. EPA, "Technical Documentation: Freeze-Thaw Conditions," U.S. Environmental Protection Agency, Washington, DC, 2023, 10 pp.

22. ASTM C39/C39M-05, "Standard Test Method for Compressive Strength of Cylindrical Concrete Specimens," ASTM International, West Conshohocken, PA, 2005, 7 pp.

23. ASTM C1231/C1231M-09, "Standard Practice for Use of Unbonded Caps in Determination of Compressive Strength of Hardened Concrete Cylinders," ASTM International, West Conshohocken, PA, 2009, 5 pp.

24. ASTM C215-19, "Standard Test Method for Fundamental Transverse, Longitudinal, and Torsional Resonant Frequencies of Concrete Specimens," ASTM International, West Conshohocken, PA, 2019, 7 pp.

25. Abate, M. S.; Evangelista, A. C. J.; and Tam, V. W. Y., "Global Research Trends in Performance-Based Structural Design: A Comprehensive Bibliometric Analysis," *Buildings*, V. 15, No. 3, Feb. 2025, Article No. 363. doi: 10.3390/buildings15030363

26. Kim, J.-H. J.; Phan, H. D.; Yi, N.-H.; Kim, S.-B.; and Jeong, H.-S., "Application of the One-Parameter Bayesian Method as the PBMD for Concrete Mix Proportion Design," *Magazine of Concrete Research*, V. 63, No. 1, Jan. 2011, pp. 31-47. doi: 10.1680/macr.2011.63.1.31

27. Kim, J.-H. J.; Phan, H. D.; Kim, B.-Y.; Choi, J.-W.; and Han, T.-S., "Development of Satisfaction Curves to Evaluate Concrete Mix Design Performance Using a Bayesian Probabilistic Method," *Construction and Building Materials*, V. 27, No. 1, Feb. 2012, pp. 578-584. doi: 10.1016/j.conbuildmat.2011.07.005

28. Phan, H. D.; Kim, J.-H. J.; Yi, N.-H.; You, Y.-J.; and Kim, J.-W., "Strength Targeted PBMD of HSC based on One-parameter Bayesian Probabilistic Method," *Journal of Advanced Concrete Technology*, V. 10, No. 4, 2012, pp. 137-150. doi: 10.3151/jact.10.137

29. Kim, T.-K.; Choi, S.-J.; Choi, J.-H.; and Kim, J.-H. J., "Prediction of Chloride Penetration Depth Rate and Diffusion Coefficient Rate of Concrete from Curing Condition Variations due to Climate Change Effect," *International Journal of Concrete Structures and Materials*, V. 13, No. 1, Dec. 2019, Article No. 15. doi: 10.1186/s40069-019-0333-4

30. Kang, S.-H.; Lee, J.-H.; Hong, S.-G.; and Moon, J., "Microstructural Investigation of Heat-Treated Ultra-High Performance Concrete for Optimum Production," *Materials*, V. 10, No. 9, Sept. 2017, Article No. 1106. doi: 10.3390/ma10091106

31. Zhang, X.; Yang, J.; Li, K.; Pu, H.; Meng, X.; Zhang, H.; and Liu, K., "Effects of Steam on the Compressive Strength and Microstructure of Cement Paste Cured Under Alternating Ultrahigh Temperature," *Cement and Concrete Composites*, V. 112, Sept. 2020, Article No. 103681.

32. Chen, F., and Qiao, P., "Probabilistic Damage Modeling and Service-Life Prediction of Concrete Under Freeze–Thaw Action," *Materials and Structures*, V. 48, No. 8, Aug. 2015, pp. 2697-2711. doi: 10.1617/s11527-014-0347-y

33. Yan, W.; Wu, Z.; Niu, F.; Wan, T.; and Zheng, H., "Study on the Service Life Prediction of Freeze–Thaw Damaged Concrete with High Permeability and Inorganic Crystal Waterproof Agent Additions Based on Ultrasonic Velocity," *Construction and Building Materials*, V. 259, Oct. 2020, Article No. 120405. doi: 10.1016/j.conbuildmat.2020.120405